Available online at www.sciencedirect.com

ScienceDirect

IFAC PapersOnline CONFERENCE PAPER ARCHIVE

IFAC PapersOnLine 54-20 (2021) 663–668

On the necessity of flexible modelling in fault detection for a flexible aircraft ⋆

Bálint Patartics * **Yağiz Kumtepe** ** **Béla Takarics** * **Bálint Vanek** *

* *Institute for Computer Science and Control. H-1111 Budapest, Kende u. 13-17., Hungary (e-mails: patartics.balint@sztaki.mta.hu, takarics.bela@sztaki.hu, vanek@sztaki.mta.hu)*

** *Roketsan Kemalpaşa 06780 Elmadağ, Ankara, Turkey (e-mail: yagiz.kumtepe@roketsan.com.tr)*

Abstract: High aspect ratio aircraft built from lighter and therefore more flexible materials are increasingly used in aviation. One of the challenges in designing a Fault Detection and Isolation (FDI) system for a flexible aircraft is to obtain an appropriate flexible model of it as opposed to rigid aircraft where modelling (or identification) is more traditional. Such a model is in general more complex and its construction requires special expertise. This paper demonstrates that fast and accurate FDI indeed necessitates the use of a flexible model but if the performance criteria can be relaxed and the sensor configuration can be changed, a rigid aircraft model can also be sufficient. Our case study revolves around an unmanned flexible aircraft built for flutter experimentation. H_∞ synthesis is used to design filters that detect the fault of the elevator actuator and the angle of attack sensor. Various sensor configurations and bandwidth specifications are used to compare the performance of the rigid and the flexible model-based designs.

Keywords: fault detection, flexible aircraft

1. INTRODUCTION

The purpose of Fault Detection and Isolation (FDI) is to develop tools with which faulty behaviour of onboard equipment can be identified. Using sensor signals, flight controller commands and possibly other data, an FDI algorithm detects faults in the actuators and sensors, e.g. stuck control surfaces or bias in the sensor measurement. An FDI solution is often part of a safety system that is capable of reconfiguring other components of the flight control system to compensate for the detected failure as described by Vanek et al. (2014).

A popular approach to FDI is to design optimal filters that estimate the difference between the actual control surface deflection and the control command, or the actual measured quantity and the sensor signal, calculating suitable residuals. (See Chen and Patton (2012)). An optimal H_∞ filter is designed by Marcos et al. (2005) to detect faults in the elevator actuator and pitch rate sensor for the Boeing 747. To use optimal filter design for FDI, an appropriate model of the aircraft is required. With the rise of flexible airframes even in commercial aviation, models that include flexible behaviour may be required for certain tasks. A flexible aircraft model is generally difficult to obtain as opposed to the classical rigid model which is usually the result of identification. The flexible model also requires more expertise to create, is generally more complex than the rigid one and it is subject to more uncertainty due to the substantial increase in model parameters. To compare the difficulties, see e.g. the construction of a flexible aircraft model by Meddaikar et al. (2019) and the classical rigid model by Beard and McLain (2012). This paper aims to give guidelines on what FDI performance requirements necessitate the use of a flexible aircraft model.

Our case study focuses on the unmanned aircraft of the FLiPASED (2019) project built for flutter control experimentation which was the subject of numerous papers, e.g. by Venkataraman et al. (2019). The airframe is depicted in Fig. 1. We want to detect two faults in the longitudinal motion of the aircraft: angle of attack sensor and elevator actuator faults. (Note that the tail of the aircraft is outfitted with ruddervators, therefore it would be more precise to say that we want to detect a fault in the ruddervators that affect the longitudinal motion of the aircraft. We will continue to refer to the control surface as elevator for simplicity.) The block diagram of the FDI filter design problem is depicted in Fig. 2. We design optimal FDI filters with different bandwidths using the rigid and the flexible model of the aircraft. Then, utilizing a simple decision mechanism, we calculate the smallest detectable fault and the detection time for each fault and for each filter. Based on these results, we make recommendations on what sensor configuration and which model to use for certain performance requirements.

The rest of the paper is structured as follows. In Section 2, the flexible and the rigid model of the aircraft is outlined along with the sensors and actuators. Section 3 describes how the optimal FDI filters are designed. The details of the performance evaluation of the filters (the calculation

⋆ The research leading to these results is part of the FLIPASED project. These projects have received funding from the Horizon 2020 research and innovation programme of the European Union under grant agreement No. 815058.

10.1016/j.ifacol.2021.11.247

Fig. 1. The demonstrator aircraft built for the FLIPASED project.

of the smallest detectable fault and detection time among others) is given in Section 4. Section 5 compares the achievable performance of the various filter designs and gives recommendations on when to use a flexible aircraft model. Finally, our findings are summarised in Section 6.

2. THE FLEXIBLE AND RIGID AIRCRAFT MODEL

The flexible aircraft, illustrated in Fig. 1, was built for flutter experimentation for the FLEXOP (2015) and subsequently for the FLiPASED (2019) H2020 projects. It is a single-engine aircraft, featuring a wing span of 7 m, aspect ratio of 20, and takeoff weight between 55 and 65 kg. The sensor and actuator configuration is illustrated in Fig. 3. Two models of this aircraft are used for filter design in this paper: a low order rigid body and a higher order flexible model. Both are linear longitudinal models obtained in straight and level flight (at 38 m/s). A detailed description is given by Takarics and Vanek (2019) and Meddaikar et al. (2019).

The outputs are the sensor signals that consist of the angle of attack (α), pitch angle (Θ), pitch rate (q), speed (V), vertical acceleration in the centre of gravity ($a_{z,\mathrm{c}}$), and the mean of the acceleration and angular rate signals from the IMU's located close to the wing tips ($a_{z,\mathrm{w}} = (a_{z,\mathrm{L}} + a_{z,\mathrm{R}})/2$, $q_{\mathrm{w}} = (q_{\mathrm{L}} + q_{\mathrm{R}})/2$, the 'w' stands for 'wing'). The sensors are modelled as first order low pass filters of the form

$$G_{\mathrm{sens}}(s) = \frac{1}{\frac{s}{2\pi\theta} + 1}, \tag{1}$$

where θ is the bandwidth. Additive white noise is assumed on the sensor outputs. Based on the documentation of the sensors and experimental data, the standard deviations of the sensor noises along with the bandwidths are listed in Table 1.

The thrust command for the engine is denoted by u_{th}. The tail control surfaces are ruddervators with the commands $u_{\mathrm{rv,L1}}$, $u_{\mathrm{rv,L2}}$, $u_{\mathrm{rv,R1}}$, and $u_{\mathrm{rv,R1}}$ in Fig. 3. These are used symmetrically, i.e. $u_{\mathrm{rv,L1}} = u_{\mathrm{rv,L2}}$ and $u_{\mathrm{rv,R1}} = u_{\mathrm{rv,R2}}$. The elevator command considered in this paper is obtained by

$$u_{\mathrm{e}} = \frac{u_{\mathrm{rv,L1}} + u_{\mathrm{rv,R1}}}{2} = \frac{u_{\mathrm{rv,L2}} + u_{\mathrm{rv,R2}}}{2}. \tag{2}$$

Thus, the input of the system is the control command $u_{\mathrm{c}} = [u_{\mathrm{e}}\ u_{\mathrm{th}}]^T$. Based on experiments, the engine dynamics can be approximated by

$$G_{\mathrm{act,th}}(s) = \frac{1}{8s + 1}. \tag{3}$$

The actuator dynamics for the elevator (for the ruddervators) is

$$G_{\mathrm{act,e}}(s) = \frac{1817}{s^2 + 54.03s + 1817}. \tag{4}$$

Since the ruddervators are transformed to a single elevator, only one actuator is included in the model. The input of the aerodynamics consists of the control surface deflection, its derivative and second derivative, hence the derivatives of the output of $G_{\mathrm{act,e}}(s)$ are also connected to the system.

The state of the system consist of the velocity components along the longitudinal and vertical axis of the body frame (u and w respectively), pitch angle (Θ), pitch rate (q), five modal coordinates and their derivatives, two lag states, and three actuator states. The frequency of the short period mode and the first bending mode of the structural dynamics have special significance in the final analysis (in Section 5). These are $\omega_{\mathrm{sp}} = 9$ rad/s and $\omega_{\mathrm{fb}} = 18$ rad/s, respectively.

The rigid aircraft model is obtained by residualising the flexible states (modal coordinates, their derivatives, and the lag states). In practice, a rigid model is usually the result of parameter identification of a standard rigid model. Our approach aims to avoid any differences between the two models that do not arise from flexibility.

3. FAULT DETECTION FILTER DESIGN

The FDI filter design is articulated as an H_∞ optimal synthesis problem similarly to the solution of Marcos et al. (2005). The generalised plant interconnection is depicted in Fig. 4. Here, $f = [f_{\mathrm{a}}\ f_{\mathrm{s}}]^T$ is the fault which is modelled as an additive disturbance on the elevator actuator command and the angle of attack measurement. The output of the FDI filter $F(s)$ is called the residual. It is the estimate of the fault signal hence it is denoted by $\hat{f} = [\hat{f}_{\mathrm{a}}\ \hat{f}_{\mathrm{s}}]^T$. The control command u_{c} is normally the output of the flight controller but since no controller is considered in the design process, it is treated as a known external disturbance.

The desired response of the residual signals to the faults is defined as

$$T_{\mathrm{des}}(s) = \frac{1}{\kappa s + 1} I_2, \tag{5}$$

where I_2 is a 2×2 identity matrix. The time constant κ is a design parameter that sets the required bandwidth (hence the speed of the response). Noise cancellation is required on the frequency range beyond the bandwidth of $T_{\mathrm{des}}(s)$. This is captured by the noise weighting function

$$W_{\mathrm{n}}(s) = R\frac{10\sqrt{2}\kappa s + 1}{\frac{\sqrt{2}\kappa}{100}s + 1}, \tag{6}$$

where R is a diagonal matrix with the standard deviations of the individual noise signals in the diagonal. The weight of the estimation error is also chosen to correspond to the bandwidth of $T_{\mathrm{des}}(s)$. It is defined as

$$W_{\mathrm{e}}(s) = \frac{0.01\kappa s + 1}{\kappa s + 1} I_2. \tag{7}$$

The weight of the input multiplicative uncertainty is

$$W_{\mathrm{u}}(s) = \frac{(s + 24.71)\left(s^2 + 121.9s + 2\cdot10^4\right)}{(s + 64.24)\left(s^2 + 138.2s + 2.6\cdot16^4\right)}. \tag{8}$$

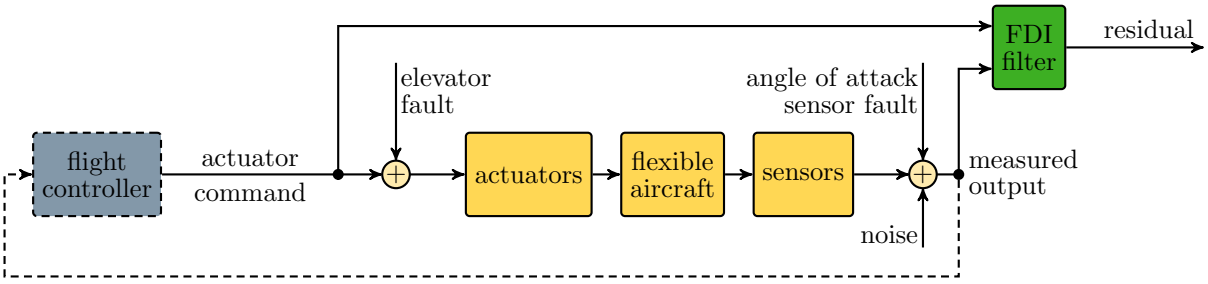

Fig. 2. Block diagram of the joint actuator and sensor fault detection problem.

Table 1. Sensor bandwidth and standard deviation of the measurement noise.

	$a_{z,\mathrm{c}}$	q	Θ	V	α	$a_{z,\mathrm{w}}$	q_{w}
type	MTI-G-710 xSense			micro Air Data System 2.0		MPU-9250	
bandwidth (θ)	200 Hz			50 Hz		200 Hz	
std. dev. of the noise	$0.08\,\mathrm{m/s^2}$	$0.3°/\mathrm{s}$	$0.6°/\mathrm{s}$	$0.33\,\mathrm{m/s}$	$0.33°/\mathrm{s}$	$0.72\,\mathrm{m/s^2}$	$5.4°/s$

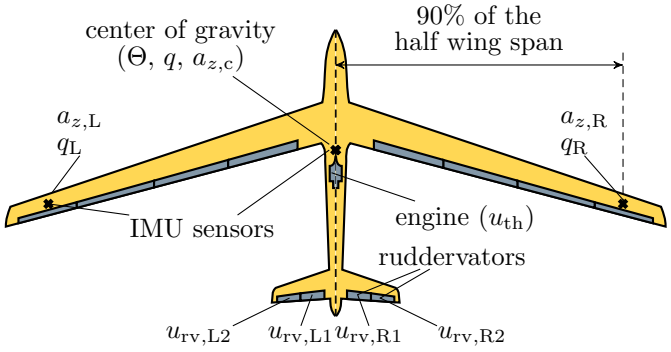

Fig. 3. Control surface configuration and sensor positions of the flexible aircraft. The control inputs and sensor signals are marked at the corresponding control surfaces and sensors.

This is chosen so that the uncertain plant

$$G_{\mathrm{plant}}(s)\,(I_2 + W_{\mathrm{u}}(s)\,\Delta(s)) \tag{9}$$

has 30% uncertainty on low frequencies, 50% at the elevator actuator bandwidth, and 100% at high frequencies. Notice that $W_{\mathrm{u}}(s)$ does not depend on κ since it describes the accuracy of the model regardless of the bandwidth requirement. These weighting functions for $\kappa = 1$ s are compared in Fig. 5.

Denote the interconnected system depicted in Fig. 4 with $F(s)$ and $\Delta(s)$ cut out by

$$\begin{bmatrix} z_\Delta \\ e \\ y_{\mathrm{m}} \\ u_{\mathrm{c}} \end{bmatrix} = M(s) \begin{bmatrix} w_\Delta \\ f \\ u_{\mathrm{c}} \\ d_{\mathrm{n}} \\ \hat{f} \end{bmatrix}. \tag{10}$$

To connect $\Delta(s)$ and $F(s)$, let us define the Linear Fractional Transformations (LFTs). For any two complex matrix (or dynamic system) $X = \begin{bmatrix} X_{11} & X_{12} \\ X_{21} & X_{22} \end{bmatrix}$ and Y, the upper LFT exists if X_{11} has the same size as Y^T and it is defined as

$$\mathcal{F}_U(X,\,Y) = X_{21}Y\,(I - X_{11}Y)^{-1}\,X_{12} + X_{22}. \tag{11}$$

Similarly, if X_{22} has the same size as Y^T, then

$$\mathcal{F}_L(X,\,Y) = X_{12}Y\,(I - X_{22}Y)^{-1}\,X_{21} + X_{11}. \tag{12}$$

The uncertain generalised plant is then

$$P(\Delta,\,s) = \mathcal{F}_U(M(s),\,\Delta(s))\,. \tag{13}$$

The objective of the design is to find a filter $F(s)$ such that the H_∞ norm of $\mathcal{F}_L(P(\Delta,\,s),\,F(s))$ is minimal for all possible uncertainties, i.e the optimisation problem is

$$\min_{F(s)} \max_{||\Delta(s)||_\infty \le 1} ||\mathcal{F}_L(P(\Delta,\,s),\,F(s))||_\infty\,. \tag{14}$$

Since $P(\Delta,\,s)$ is robustly stable (stable for all admissible $\Delta(s)$), this is equivalent to

$$\min_{F(s)} ||\mathcal{F}_L(M(s),\,F(s))||_\infty\,. \tag{15}$$

This optimization is solved using the standard H_∞ synthesis tool implemented in the `hinfsyn` function of MATLAB. For details about the robust design technique, see Skogestad and Postlethwaite (2007).

4. EVALUATION OF THE FAULT DETECTION PERFORMANCE

For the evaluation of the FDI filter, the weighting functions and performance output channels are removed from the generalized plant in Fig. 4. Hence, we consider the interconnection in Fig. 6. Here, $F(s)$ is the filter designed by the process described in Section 3. Let us denote the system in Fig. 6 by

$$\hat{f} = T(\Delta,\,s) \begin{bmatrix} f \\ u_{\mathrm{c}} \\ n \end{bmatrix} \tag{16}$$

For simplicity, we only describe the tools we use to evaluate the performance of the actuator fault detection. The calculations employed for the sensor fault detection evaluation are identical. The theoretical background of the computations involved in this section is described by Skogestad and Postlethwaite (2007).

The effect of the control command on the residual is measured by the worst-case gain of $T(\Delta,\,s)$ from the input u_{c} to the output f_{a}. Denote this gain by

$$\vartheta_{\mathrm{a}} = \max_{||\Delta(s)||_\infty \le 1} \left|\left| T_{\hat{f}_{\mathrm{a}} \leftarrow u_{\mathrm{c}}}(\Delta,\,s)\,\Lambda_u \right|\right|_\infty, \tag{17}$$

where $\Lambda_u = \mathrm{diag}(15°,\,0.2)$ is a scaling matrix that represents the maximum control input. We use the approximation that if there is no noise and fault in the system (i.e. $n = 0$ and $f = 0$), then the residual produced by the control command alone is at most ϑ_{a} (i.e. $\hat{f}_a \le \vartheta_{\mathrm{a}}$) for all admissible values of the uncertainty $\Delta(s)$. Note that

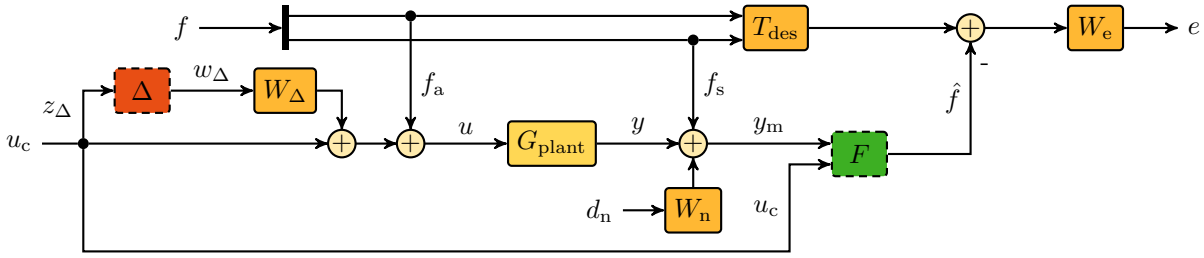

Fig. 4. Generalized plant interconnection for the H_∞ FDI filter design.

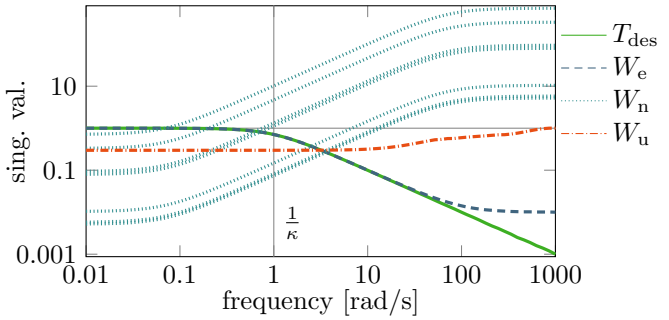

Fig. 5. Weighting functions used for the H_∞ synthesis. The value of the design parameter is $\kappa = 1$ s. (Since the standard deviations of the noise channels are different, $W_n(s)$ is represented by multiple lines.)

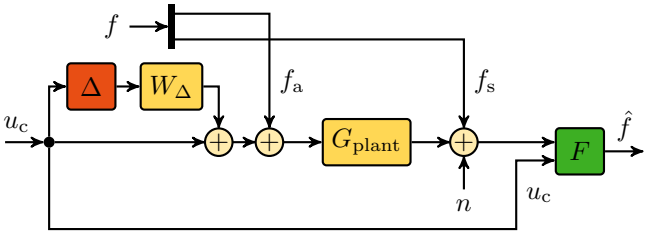

Fig. 6. Interconnection of the uncertain aircraft model and the H_∞ FDI filter design used in the performance evaluation.

strictly speaking, instead of the H_∞ norm, the induced L_∞ should be used. However, the induced L_∞ norm is difficult to compute in the presence of uncertainty. Also, these two norms bound each other up to a constant factor, therefore trends we want to observe are not influenced by the choice of the norm.

The effect of the noise on the residual is captured by the standard deviation of $\hat{f}_a$ due to the noise. This is calculated as the H_2 norm of $T(\Delta,\, s)$ from n to $\hat{f}_a$, i.e.

$$\sigma_a^2 = \left\| T_{\hat{f}_a \leftarrow n}(0,\, s)\, R \right\|_2 . \tag{18}$$

Recall that R is a diagonal matrix with the standard deviations of the noise signals on the diagonal. We use $\Delta(s) = 0$ to indicate that the value of $\Delta(s)$ is arbitrary in this computation since our model assumes no uncertainty in the system in the channels from the noise to the residual.

The above quantities are used to define the detection time and the smallest robustly detectable fault. We use a simple threshold decision logic to decide whether a fault actually occurred. In the practical implementation of an FDI system, an integration-based or an up-down counter-based decision logic is usually used as described by Ossmann and Pusch (2019), and Wheeler (2011) respectively. Our simple threshold logic approximates the behavior of those more

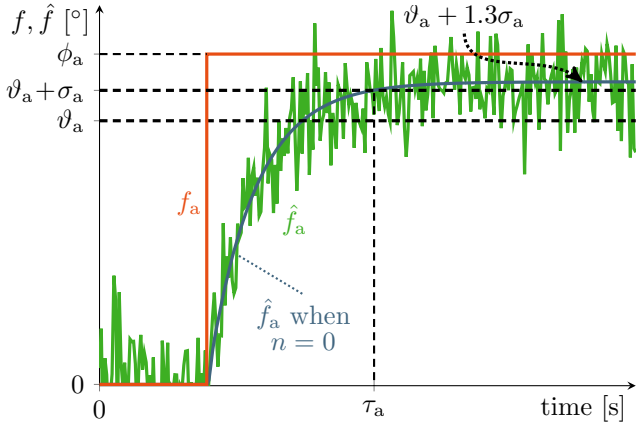

Fig. 7. Definition of the detection time and smallest detectable fault.

complex solutions. The decision threshold is the maximum residual caused by the control input plus one standard deviation of the residual signal, i.e. $\vartheta_a + \sigma_a$.

If the residual is $\vartheta_a + 1.3\sigma_a$ in steady-state and without noise, then the probability that $\hat{f}_a > \vartheta_a + \sigma_a$ in the presence of noise is 90%. Therefore, we call the fault corresponding to this residual the smallest robustly detectable fault. It is denoted by ϕ_a and is defined by the equation

$$T_{\hat{f}_a \leftarrow f_a}(0,\, 0)\, \phi_a = \vartheta_a + 1.3\sigma_a. \tag{19}$$

Note that similarly to the noise, there is no uncertainty in the channels form f to $\hat{f}$. Therefore, the uncertainty sample $\Delta(s) = 0$ is used again in the computations. In accordance with the definition of ϕ_a, the detection time τ_a is defined as the time when the step response of $T_{\hat{f}_a \leftarrow f_a}(0,\, s)\, \phi_a$ crosses the threshold $\vartheta_a + \sigma_a$. These quantities are illustrated in Fig. 7.

To contrast the results with frequency domain data, we also define the bandwidth of the FDI filter $F(s)$. We define the bandwidth as the frequency above which the singular value of the filter to the $\hat{f}_a$ output channel is less than -6 dB. I.e. B_a is the bandwidth of $F_{\hat{f}_a}(s)$ if $\bar{\sigma}(F_{\hat{f}_a}(j\omega)) < -6$ dB for $\omega > B_a$. This definition means that almost all of the frequency content of $\hat{f}_a$ is concentrated in the frequency interval $[0,\, B_a]$.

Finally, we demonstrate these analysis metrics by evaluating the filter design for $\kappa = 0.5$ s and $\kappa = 0.2$ s. For this filter design, we use the measurements α, Θ, q, V, and $a_{z,c}$. (A detailed evaluation for multiple values of κ and different sensor configurations is presented in Section 5.)

When $\kappa = 0.5$ s, the resulting filter bandwidths are $B_a = 3.11$ rad/s and $B_s = 3.41$ rad/s. At these frequencies, the model uncertainty is still low, therefore design conditions

can be met. The effect of the control input to the residuals is $\vartheta_a = 4.08°$ and $\vartheta_s = 0.06°$. Since f_a acts on the input of the system and the input dynamics are uncertain, ϑ_a is much greater than ϑ_s. The noise on the other hand affects the estimation of f_s more. This is reflected by the values $\sigma_a = 2.62°$ and $\sigma_s = 4.35°$. The smallest detectable faults and detection times are $\phi_a = 8.16°$, $\phi_s = 5.67°$, $\tau_a = 1.16$s, and $\tau_s = 0.78$ s. According to both performance measures, the sensor fault detection problem proves easier to solve. If we conduct this analysis using the filter designed for the rigid model, we get $\phi_a = 8.21°$, $\phi_s = 5.90°$, $\tau_a = 1.17$ s, and $\tau_s = 0.81$s. These values are very close to the previous ones therefore we can conclude that if this performance is satisfactory to our goals, it is sufficient to carry out the filter design using the rigid model.

If $\kappa = 0.2$ s however, the difference is greater for the actuator fault estimation. In this case, the bandwidths are higher: $B_a = 7.96$ rad/s and $B_s = 8.54$ rad/s. This causes the detection time to decrease to $\tau_a = 0.41$ s and $\tau_s = 0.31$s. This is achieved at the cost of lower sensitivity to the faults which is expressed by the increase in the smallest detectable faults: $\phi_a = 11.16°$ and $\phi_s = 7.08°$. When the filter is designed for the rigid model, these values become $\tau_a = 0.55$ s, $\tau_s = 0.32$ s, $\phi_a = 13.57°$ $\phi_s = 7.59°$. At this bandwidth, the rigid and flexible models are more different than in the previous case (for $\kappa = 0.5$s) therefore the difference between the performance measures are more pronounced. The degradation is especially significant for the actuator fault estimation.

5. COMPARISON OF THE RIGID AND FLEXIBLE MODEL BASED DESIGNS

In this section, we compare the FDI filters designed for the rigid and flexible aircraft models. The performance metrics we consider are the detection time, smallest detectable fault and filter bandwidth as defined in Section 4. In order to study the usefulness of acceleration measurements (and q_w), three sensor configurations are compared:

no acc.: α, Θ, q, V
acc.: α, Θ, q, V, $a_{z,c}$
acc. +w: α, Θ, q, V, $a_{z,c}$, $a_{z,w}$, q_w.

Our calculations revealed that the accelerometers placed close to the wing tips do not improve FDI performance since there is no difference in performance between the configurations labelled 'acc.' and 'acc. +w'. Hence, we only compare configuration 'no acc.' and 'acc.' in the rest of this section. Figs. 8-13 present the data that are the basis of the comparison. Each figure has graphs that corresponds to the flexible and rigid model-based designs (flex. and rigid) and to sensor configuration 'no acc.' and 'acc'.

Fig. 8 presents the trade-off between the smallest detectable fault and the detection time for the actuator fault detection. If accelerometer measurements are used, the performance of the filters designed for the rigid and flexible models are very similar for $\tau_a \geq 0.8$ s. If we aim to achieve lower detection time than 0.8 s, then a flexible model is clearly required, since the performance curves diverge in this domain. In terms of filter bandwidth, this divergence in observable above half of the frequency of the shot period mode ($\omega_{sp}/2$) in Figs. 9 and 10.

Without accelerometer measurements, the achievable performance is strictly worst but it is not affected by the choice of design model so heavily. There is noticeable

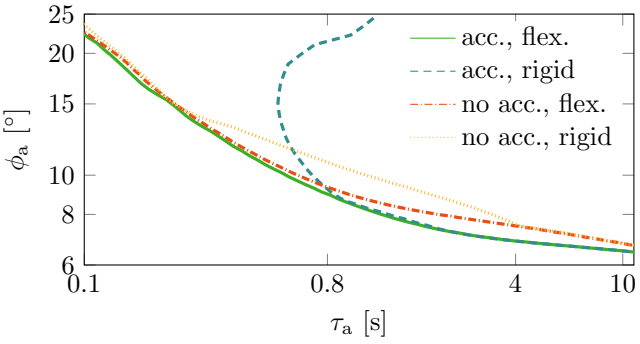

Fig. 8. Trade-off between the smallest detectable fault and the detection time for the actuator fault detection.

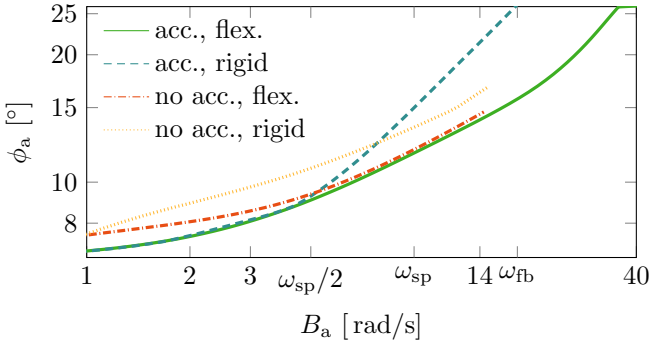

Fig. 9. Comparison of the smallest detectable actuator faults as a function of filter bandwidth.

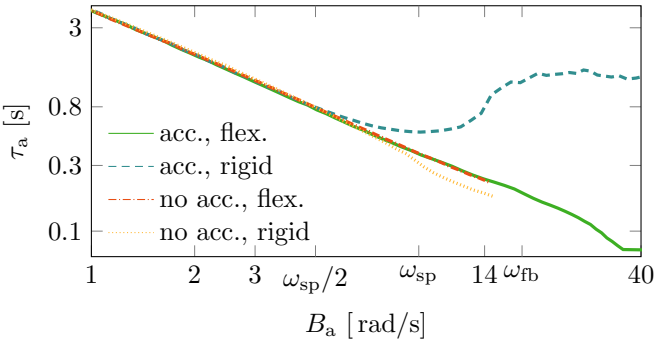

Fig. 10. Comparison of the detection times of the actuator fault detection as a function of filter bandwidth.

difference between the two 'no acc.' curves in Fig. 8 but the difference is less pronounced. As demonstrated by Fig. 9, there is only a couple of degrees difference between the smallest detectable fault in the two cases. However, this difference persists on the entire bandwidth range of interest. On the other hand, the detection times are very close as illustrated in Fig. 10. The ϕ_a and τ_a values are only plotted up to around 14 rad/s (close to ω_{fb}) because further improvement in the performance requires more than 60 rad/s filter bandwidth. (The corresponding data points are still shown in Fig. 8, however.) This discontinuity occurs, because the lack of $a_{z,c}$ measurement hides the high frequency behaviour of the aircraft which results in a local peak in the filter gain that tends towards high frequencies. This local peak becomes prominent (greater than -6 dB) at around 60 rad/s, causing the filter bandwidth to jump above 60 rad/s.

The angle of attack sensor fault estimation is not affected as much by the model uncertainty and flexibility as the

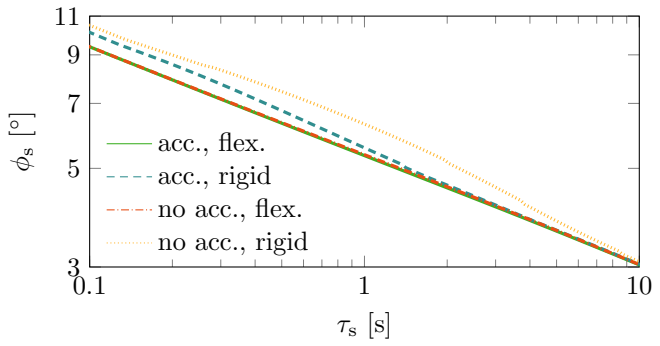

Fig. 11. Trade-off between the smallest detectable fault and the detection time for the sensor fault detection.

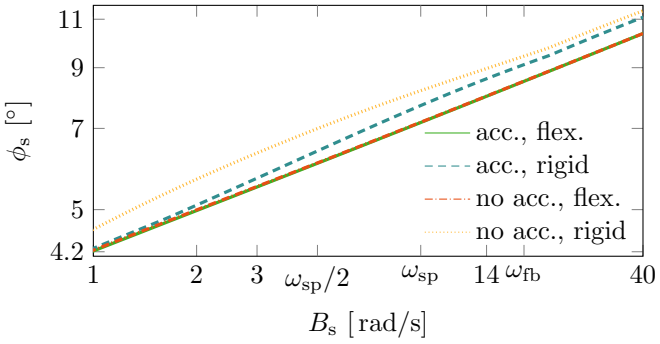

Fig. 12. Comparison of the smallest detectable sensor faults as a function of filter bandwidth.

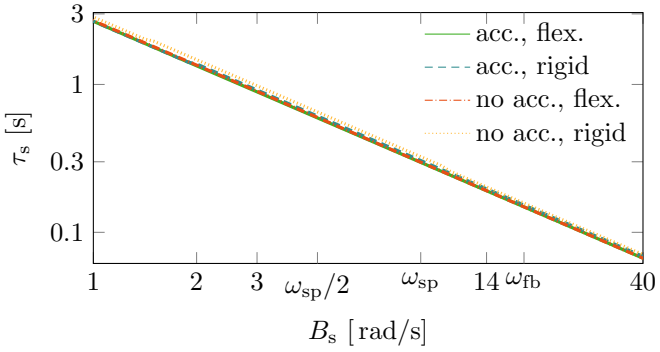

Fig. 13. Comparison of the detection times of the sensor fault detection as a function of filter bandwidth.

elevator actuator fault. Hence, faster and more precise fault detection is attainable overall. For low filter bandwidths (high detection times), the ϕ_s and τ_s values are very close for all four options in Figs 11-13. Similarly to the elevator fault detection, the difference between flexible and rigid model-based designs only show if we aim for low detection times. The difference however, is small (less than one degree) for the domain of our analysis. The worst performance clearly corresponds to the case when no acceleration measurement is used and the filter is designed for the rigid model. But since the performance measures track close to each other for all four cases, we conclude that the performance of the angle of attack sensor fault detection is not impacted greatly by the choice of design model or sensor configuration.

6. CONCLUSIONS

Using a specific case study, guidelines are established on when a flexible model is required for FDI filter design for a flexible aircraft. It is concluded that only minor performance improvement is attainable for the angle of attack sensor FDI with the involvement of the flexible model. In contrast, the elevator FDI is greatly impacted by the choice of sensor configuration and design model. If good performance is expected at high frequencies (beyond the frequency of the first bending mode), then both acceleration measurement at the center of gravity and the flexible model are required. Still using the acceleration measurement, good performance is achieved using the rigid model up to half of the frequency of the short period mode. At the cost of some loss in accuracy, a design based on the rigid model is capable of providing acceptable performance up the frequency of the first bending mode if the acceleration measurement is not used.

REFERENCES

Beard, R.W. and McLain, T.W. (2012). *Small unmanned aircraft: Theory and practice.* Princeton university press.

Chen, J. and Patton, R. (2012). *Robust Model-Based Fault Diagnosis for Dynamic Systems.* The International Series on Asian Studies in Computer and Information Science. Springer US.

FLEXOP (2015). *Flutter Free FLight Envelope eXpansion for ecOnomical Performance improvement, Horizon 2020 research and innovation programme of the European Union, grant agreement No 636307.* URL `https://flexop.eu/, Accessed on 11. 2019.`

FLiPASED (2019). *Flight Phase Adaptive Aero-Servo-Elastic Aircraft Design Methods, Horizon 2020 research and innovation programme of the European Union, grant agreement No 815058.* URL `https://flipased.eu/, Accessed on 03. 2021.`

Marcos, A., Ganguli, S., and Balas, G.J. (2005). An application of H_∞ fault detection and isolation to a transport aircraft. *Control Engineering Practice*, 13(1), 105–119.

Meddaikar, Y.M., Dillinger, J., Klimmek, T., Krueger, W., W uestenhagen, M., Kier, T.M., Hermanutz, A., Hornung, M., Rozov, V., Breitsamter, C., et al. (2019). Aircraft aeroservoelastic modelling of the FLEXOP unmanned flying demonstrator. In *AIAA Scitech 2019 Forum*, 1815.

Ossmann, D. and Pusch, M. (2019). Fault tolerant control of an experimental flexible wing. *Aerospace*, 6(7), 76.

Skogestad, S. and Postlethwaite, I. (2007). *Multivariable feedback control: analysis and design*, volume 2. Citeseer.

Takarics, B. and Vanek, B. (2019). Tensor product model-based robust flutter control design for the FLEXOP aircraft. *IFAC-PapersOnLine*, 52(12), 134–139. 21st IFAC Symposium on Automatic Control in Aerospace ACA 2019.

Vanek, B., Edelmayer, A., Szabó, Z., and Bokor, J. (2014). Bridging the gap between theory and practice in LPV fault detection for flight control actuators. *Control Engineering Practice*, 31, 171–182.

Venkataraman, R., Bauer, P., Seiler, P., and Vanek, B. (2019). Comparison of fault detection and isolation methods for a small unmanned aircraft. *Control Engineering Practice*, 84, 365–376.

Wheeler, T.J. (2011). *Probabilistic performance analysis of fault diagnosis schemes.* Ph.D. thesis, UC Berkeley.